SAND2023-04292C

Sandia National Laboratories

# Development of a Ductile Rupture Failure Surface for a High-Strength Steel Using the Xue-Wierzbicki Failure Model

John L. Bignell

Robert J. Kalan

Douglas J. Ammerman

The International Symposium on the Packaging and Transportation of Radioactive Materials (PATRAM)

Juan-les-Pins, Antibes, France

June 11-15, 2023

Sandia National Laboratories is a multimission laboratory managed and operated by National Technology & Engineering Solutions of Sandia, LLC, a wholly owned subsidiary of Honeywell International Inc., for the U.S. Department of Energy's National Nuclear Security Administration under contract DE-NA0003525.

Sandia National Laboratories is a multimission laboratory managed and operated by National Technology & Engineering Solutions of Sandia, LLC, a wholly owned subsidiary of Honeywell International Inc., for the U.S. Department of Energy's National Nuclear Security Administration under contract DE-NA0003525.

# Introduction

- Sandia National Laboratories (SNL) has developed a hazardous materials transportations package that satisfies Title 10 of the U.S. Code of Federal Regulations, Part 71 (10 CFR 71).
  - 10 CFR 71 requires that the package contain the hazardous material in the event of an accident, and
  - Defines hypothetical accident conditions (HAC) for used in design: Including 129 m/s impact.
- Containment is achieved in the package using a precipitation hardened stainless steel containment vessel (CV).
  - PH13-8Mo H950 or UNS13800
- To assess the CV for ductile rupture under HAC conditions, parameters for the Xue-Wierzbicki (X-W) failure model have been developed for PH13-8Mo H950.
- This presentation describes the mechanical testing and finite element analyses completed to develop the X-W failure model parameters.

# Rupture in Ductile Metals

- Early work by Bridgman demonstrated a dependence of the fracture strain ($\bar{\varepsilon}_f$) of ductile metals on stress triaxiality ($\eta = \sigma_m/\bar{\sigma}$):

$$\bar{\varepsilon}_f = C_1 + C_2 \exp(C_3\eta)\,,$$

  where the mean stress ($\sigma_m = I_1/3$) is proportional to the first stress invariant ($I_1$), and the von Mises equivalent stress ($\bar{\sigma} = \sqrt{3J_2}$) is proportional to the second invariant of the deviatoric stress tensor ($J_2$).

- More recently, the importance of including dependence of the fracture strain on the third invariant of the deviatoric stress tensor ($J_3$) has been recognized.

- The X-W failure model includes dependence on $J_3$ through a variable called the deviatoric state parameter ($\xi = \cos(3\theta) = 27J_3/2\bar{\sigma}^3$).

# X-W Failure Model

- The X-W model postulates that fracture will occur when the accumulated plastic strain ($\bar{\varepsilon}$), modified be a function $F(\eta, \xi)$, reaches a limiting value of one.

$$\int_0^{\bar{\varepsilon}_f} \frac{\mathrm{d}\bar{\varepsilon}}{F(\eta, \xi)} = 1$$

- Because the stress triaxiality and deviatoric state parameter vary during loading, average values of the parameters are required to define a failure surface.

$$\eta_{av} = \frac{1}{\bar{\varepsilon}_f} \int_0^{\bar{\varepsilon}_f} \eta(\bar{\varepsilon}) \mathrm{d}\bar{\varepsilon} \qquad \xi_{av} = \frac{1}{\bar{\varepsilon}_f} \int_0^{\bar{\varepsilon}_f} \xi(\bar{\varepsilon}) \mathrm{d}\bar{\varepsilon}$$

- Evaluation of the failure integral using the average stress triaxiality and deviatoric parameter yields $\bar{\varepsilon}_f = F(\eta_{av}, \xi_{av})$.

# X-W Failure Model

- The X-W model assumes that the fracture strain is bounded above by an axisymmetric stress state ($\xi_{av} = 1$) curve ($\bar{\varepsilon}_f^{ax}$) and below by a plane strain ($\xi_{av} = 0$) curve ($\bar{\varepsilon}_f^{ps}$).

$$\bar{\varepsilon}_f^{ax} = C_1 \mathrm{e}^{-C_2 \eta_{av}} \text{ for } \xi_{av} = 1, \quad \bar{\varepsilon}_f^{ps} = C_3 \mathrm{e}^{-C_4 \eta_{av}} \text{ for } \xi_{av} = 0$$

- The X-W model also assumes an elliptic functional dependence of $\bar{\varepsilon}_f$ on $\xi$.

$$\left( \frac{\bar{\varepsilon}_f^{ax} - \bar{\varepsilon}_f}{\bar{\varepsilon}_f^{ax} - \bar{\varepsilon}_f^{ps}} \right)^{1/m} + \xi^{1/m} = 1$$

where $m$ is the closest even integer to $1/n$ and $n$ is the power law hardening exponent for the material. Taken together, the fracture strain may be defined as follows.

$$\bar{\varepsilon}_f = C_1 \mathrm{e}^{-C_2 \eta_{av}} - (C_1 \mathrm{e}^{-C_2 \eta_{av}} - C_3 \mathrm{e}^{-C_4 \eta_{av}}) \left(1 - \xi^{1/n}\right)^n$$

# Material Testing

- Mechanical tests were conducted at both 20 °C and -40 °C to collect the data needed to build a X-W fracture model for PH13-8Mo H950.
- Five test specimens of differing stress triaxiality and deviatoric state parameter were used in the test campaign.
- All test specimens were extracted from a cylindrical ring of material with their primary tensile axis oriented parallel to the axis of the cylinder.
- R5 specimens included radial & axial samples.

| Specimen Name | Stress Triaxiality (η) | Deviatoric State Parameter (ξ) |
|---|---|---|
| **R5** | ~0.66 | ~1.0 |
| **9 mm Notch** | ~0.75 | ~1.0 |
| **3 mm Notch** | ~0.95 | ~1.0 |
| **Flat-Groove** | ~0.55 | ~0.0 |
| **Shear** | ~0.00 | ~0.0 |

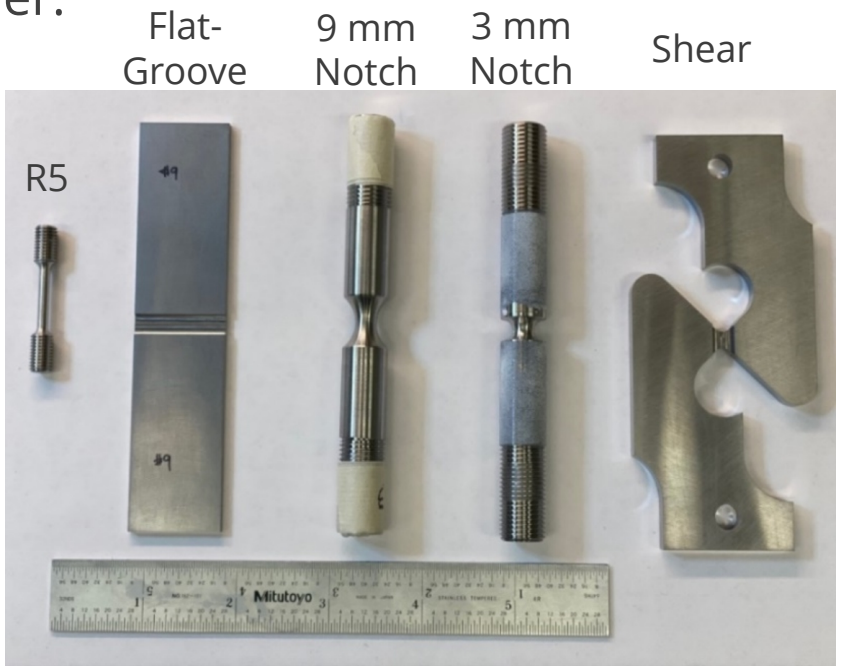

# Material Testing

- All specimens tested in uniaxial tension using a servo hydraulic load frame.
- Applied load was measured using a 260 MN load cell, sub-ranged for specific tests to give more force precision.
- An environmental chamber used to perform testing at -40 °C.
- Strain measured during testing using digital image correlation (DIC).
- Samples were loaded at rates between 0.008 mm/sec and 0.012 mm/sec depending on specimen type.
- Post-test optical and scanning electron microscopy (SEM).

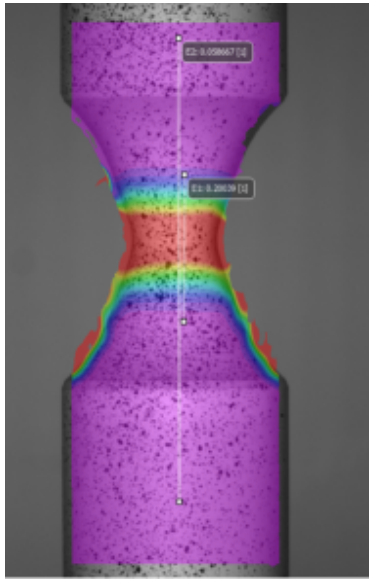

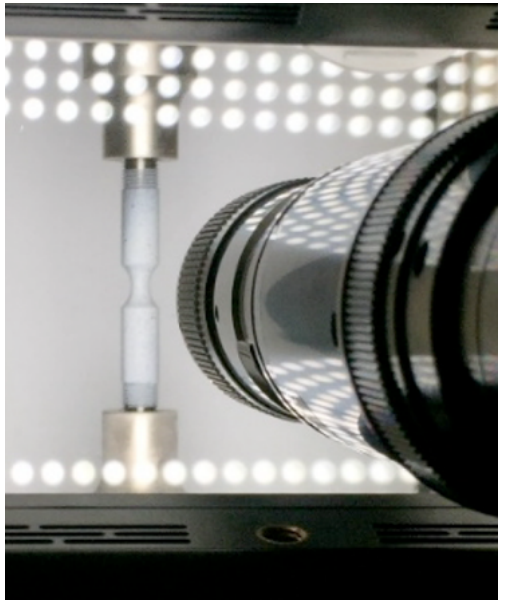

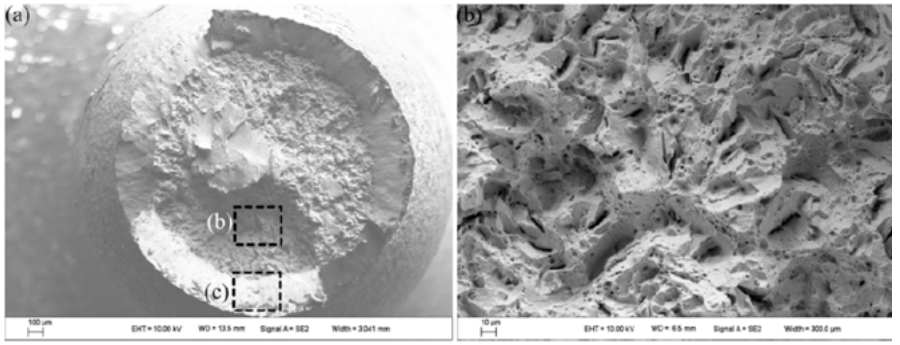

# Material Testing Results

- R5 specimen testing showed minor differences in mechanical properties between the radial and axial directions.
- Moderate temperature dependence was observed in the response of all specimens.
  - YS and UTS typically 3% to 6% higher at lower temperature, and
  - Ductility and RA 4% to 16% lower at lower temperature.
- Ductile, cup and cone fracture surfaces observed at both temperatures.
- A notable exception: 3 mm notch test specimen results.
  - UTS and YS at -40 °C were 4% to 5% greater than at 22 °C, but
  - Ductility was 66% lower and RA was 75% lower.

| Specimen Type | Temp. | Modulus of Elasticity (E) | Yield Stress (YS) | Ultimate Tensile Strength (UTS) | Ductility | Average Reduction in Area (RA) |
|---|---|---|---|---|---|---|
| | °C | GPa | MPa | MPa | % | % |
| R5 Axial | 22 | 181 ± 1 | 1430 ± 22.7 | 1570 ± 16.0 | 12.8 ± 0.9 | 57.4 |
| | -40 | 182 ± 4 | 1490 ± 7.9 | 1640 ± 3.7 | 12.0 ± 0.4 | 55.0 |
| R5 Radial | 22 | 185 ± 1 | 1470 ± 13.0 | 1600 ± 6.4 | 12.1 ± 0.3 | 55.7 |
| | -40 | 186 ± 5 | 1530 ± 31.8 | 1660 ± 7.8 | 11.9 ± 0.7 | 48.6 |
| 9 mm Notch | 22 | - | 1760 ± 1.4 | 1810 ± 1.8 | 5.6 ± 0.5 | 42.8 |
| | -40 | - | 1820 ± 4.7 | 1900 ± 8.5 | 4.9 ± 0.8 | 31.6 |
| 3 mm Notch | 22 | - | 1850 ± 37.1 | 2070 ± 6.9 | 7.6 ± 0.8 | 23.5 |
| | -40 | - | 1930 ± 30.9 | 2170 ± 15.4 | 2.6 ± 0.3 | 5.8 |
| Flat-Groove | 22 | - | 1500 ± 63.9 | 1740 ± 14.8 | 7.3 ± 0.1 | - |
| | -40 | - | 1410 ± 52.9 | 1840 ± 6.8 | 7.7 ± 0.5 | - |

# R5 Specimen Results

- Optical and SEM imaging of the fracture surfaces showed typical cup and cone fracture in all specimens, including those tested at -40 °C.
- Cross-sections taken of the fracture surface show the presence of voids up to 500 μm below the fracture surfaces, indicating failure by void nucleation, growth, and coalescence.

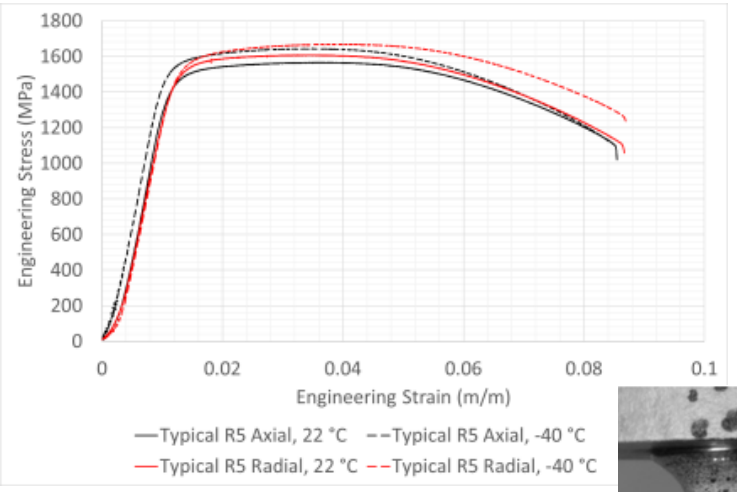


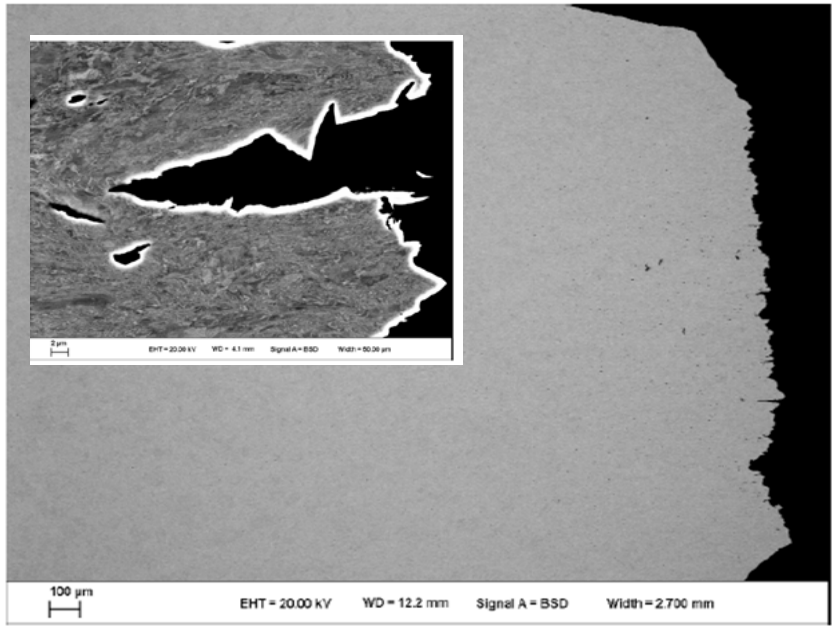


22 °C

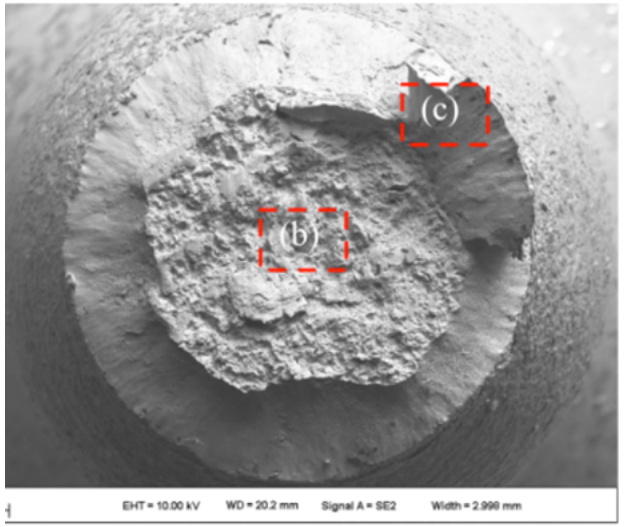


-40 °C

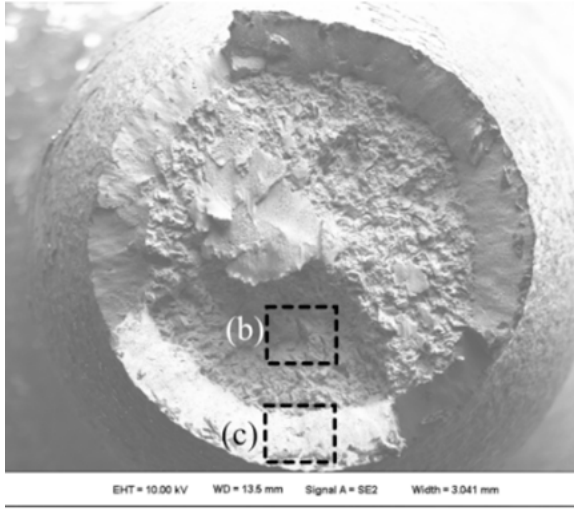


# 3 mm Notch Specimen Results

- The 3 mm notch test specimens exhibited significantly different mechanical behaviors at the two tested temperatures.
- Fracture surfaces of samples tested at 22 °C suggest ductile fracture, exhibiting cup and cone type failure.
- Samples tested at -40 °C suggest ductile fracture, but also exhibit features reminiscent of brittle failure including indications of trans-granular fracture and significantly smaller shear lips.
- This suggest that the ductile-to-brittle transition temperature for PH13-8Mo H950 is near -40 °C.

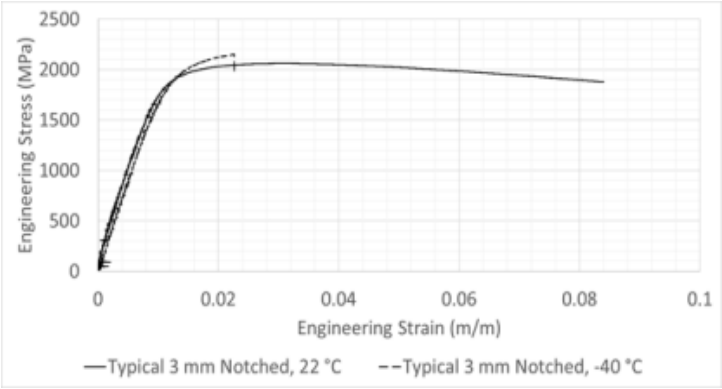


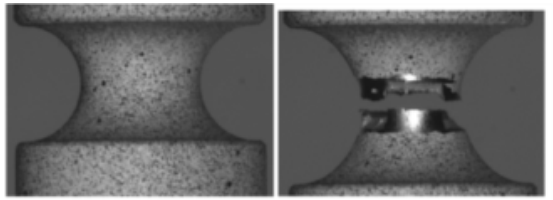

| Specimen Type | Temp. | Yield Stress (YS) | Ultimate Tensile Strength (UTS) | Ductility | Average Reduction in Area (RA) |
|---|---|---|---|---|---|
| | °C | MPa | MPa | % | % |
| 3 mm Notch | 22 | 1850 ± 37.1 | 2070 ± 6.9 | 7.6 ± 0.8 | 23.5 |
| | -40 | 1930 ± 30.9 | 2170 ± 15.4 | 2.6 ± 0.3 | 5.8 |

22 °C

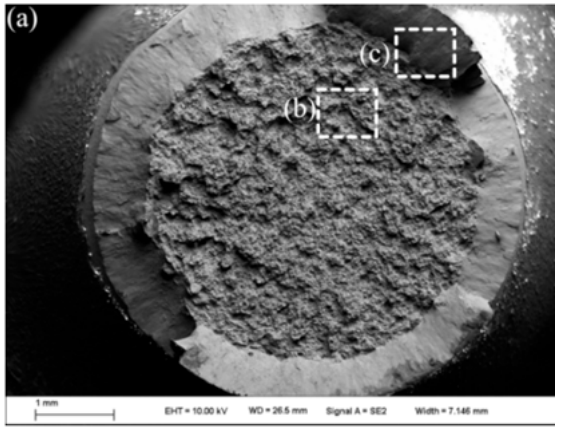


-40 °C

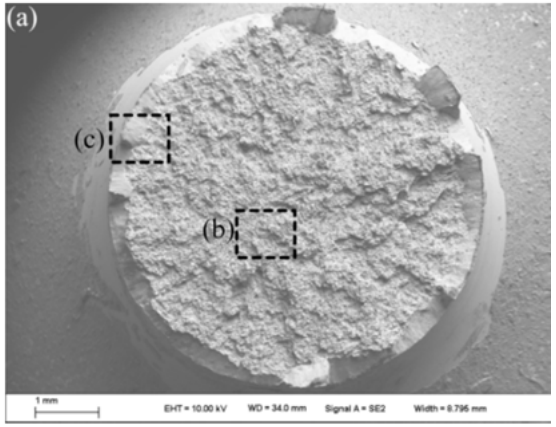

# Flat-Grooved Specimen Results

- The YS varied significantly (±4%) specimen-to-specimen so it is not possible to conclude if YS varied with temperature.
- Strain across the width of the specimen varied significantly, with the strains differing across the width by 3% to 4%.
- Full-field strain data indicate strain localization would occur on one side of the sample before fracture.
- Little difference was observed in the fracture surfaces of samples tested at both temperatures.

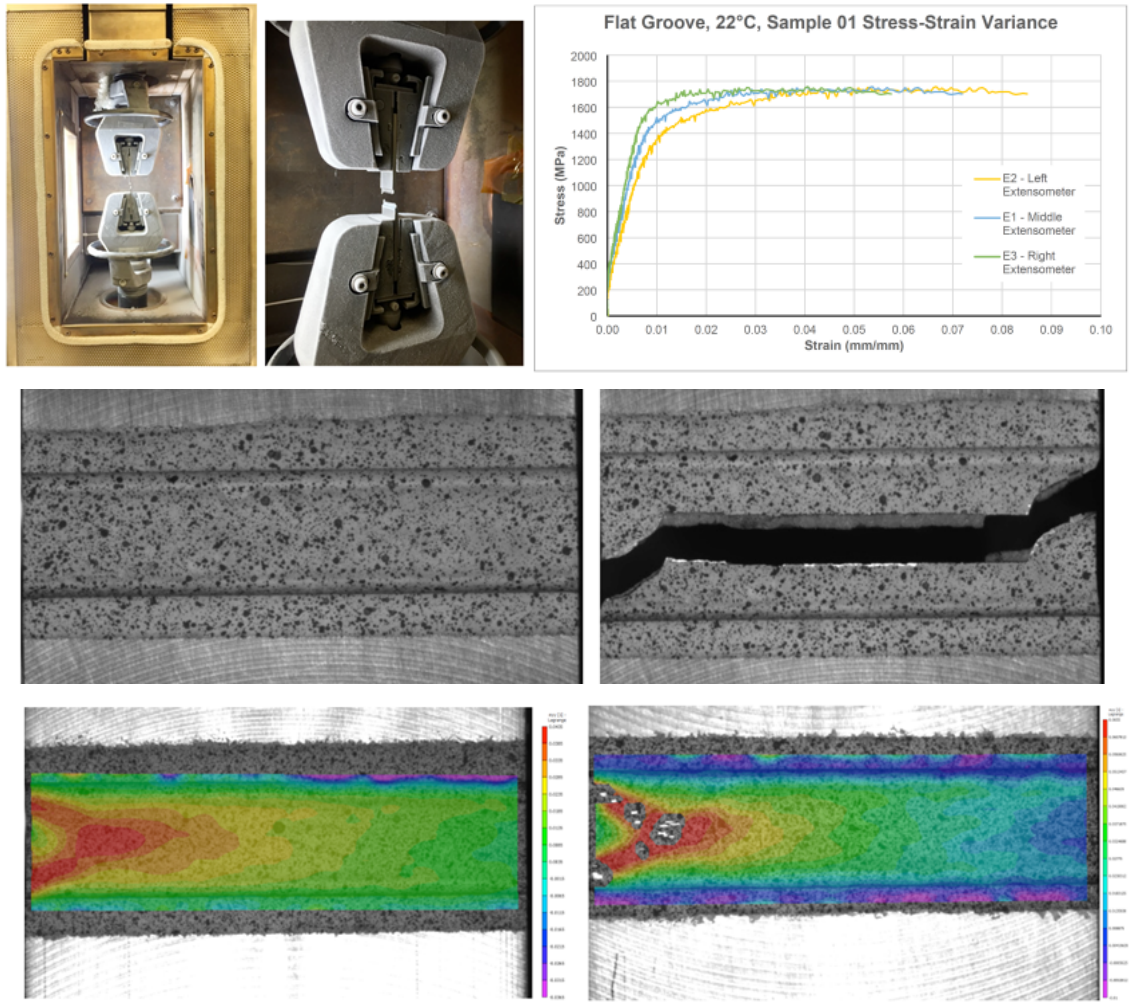

# Finite Element Analyses

- Finite element analyses were completed to extract the necessary information from the material test data to develop a X-W failure surface at room temperature and -40 °C.
- This consisted of a three-step process at each temperature.
  1. Hardening curves were developed by matching the response of a finite element model (FEM) with data from the R5 specimen tests.
  2. Using the hardening curves developed in the first step, FEM simulations of the remaining four specimen tests were completed and the relevant failure parameters extracted.
  3. Using the failure quantities derived in the second step, the four free parameters in the fracture strain equation were determined for each temperature.

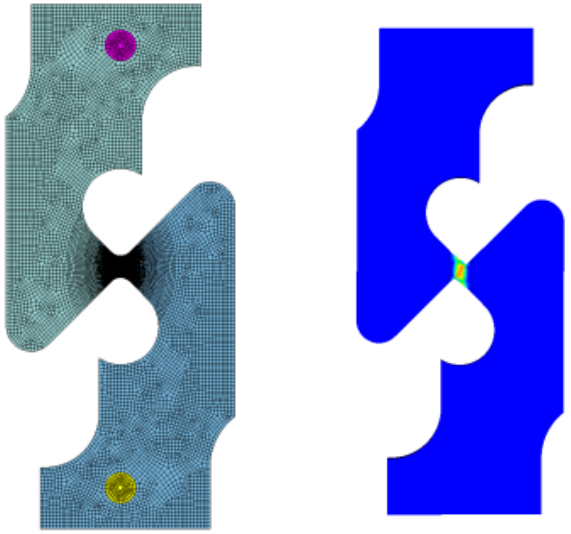



| Specimen Name | 20 °C | | | -40 °C | | |
|---|---|---|---|---|---|---|
| | Stress Triaxiality (η) | Deviatoric State Parameter (ξ) | Equivalent Plastic Strain at Failure | Stress Triaxiality (η) | Deviatoric State Parameter (ξ) | Equivalent Plastic Strain at Failure |
| **R5** | 0.593 | 1.0 | 0.892 | 0.605 | 1.0 | 0.867 |
| **9 mm Notch** | 0.785 | 1.0 | 0.520 | 0.767 | 1.0 | 0.296 |
| **3 mm Notch** | 1.095 | 1.0 | 0.190 | 0.878 | 1.0 | 0.018 |
| **Flat-Groove** | 0.578 | 0.0 | 0.194 | 0.556 | 0.0 | 0.078 |
| **Shear** | 0.0031 | 0.0 | 0.475 | 0.0033 | 0.0 | 12 |

# Finite Element Analyses Results

- Three tests with a ξ=1 were performed and only two are required to determine C1 and C2.
- At 20 °C and ξ=1 the assumed exponential fit to all three data points is good, so the differences in C1 and C2 coefficients are minimal, regardless of which two data points are used to determine the coefficients.
- At -40 °C and ξ=1 the assumed exponential fit to all three data points is not good, which results in significant variation in C1 and C2 based on which two sets of data are used.
- Assumed exponential relationship at ξ=1 may not be valid for this material at -40 °C at high stress triaxiality (ξ>0.8) applicable to the 3 mm notch specimens.

$$\bar{\varepsilon}_f^{ax} = C_1 e^{-C_2 \eta_{av}}$$

$$\bar{\varepsilon}_f = C_1 e^{-C_2 \eta_{av}} - \left(C_1 e^{-C_2 \eta_{av}} - C_3 e^{-C_4 \eta_{av}}\right)\left(1 - \xi^{1/n}\right)^n$$

| Temperature (°C) | n | m | C1 and C2 Parameter Source | C1 | C2 | C3 | C4 |
|---|---|---|---|---|---|---|---|
| **20** | 0.3488 | 2 | R5, 3 mm | 5.550 | 3.084 | 0.477 | 1.552 |
| | | | R5, 9 mm | 4.716 | 2.809 | 0.477 | 1.552 |
| | | | 9 mm, 3 mm | 6.687 | 3.254 | 0.477 | 1.552 |
| **-40** | 0.3607 | 2 | R5, 3 mm | 4495.440 | 14.148 | 0.493 | 3.309 |
| | | | R5, 9 mm | 62.463 | 7.074 | 0.493 | 3.309 |
| | | | 9 mm, 3 mm | 1.093e+07 | 23.030 | 0.493 | 3.309 |

# Derived Failure Surfaces

| | R5 & 3 mm Notch | R5 & 9 mm Notch | 9 mm & 3 mm Notch |
|---|---|---|---|
| 20 °C | 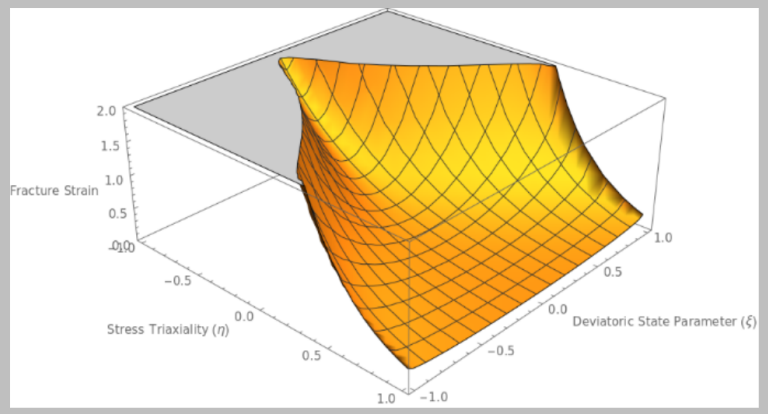 | 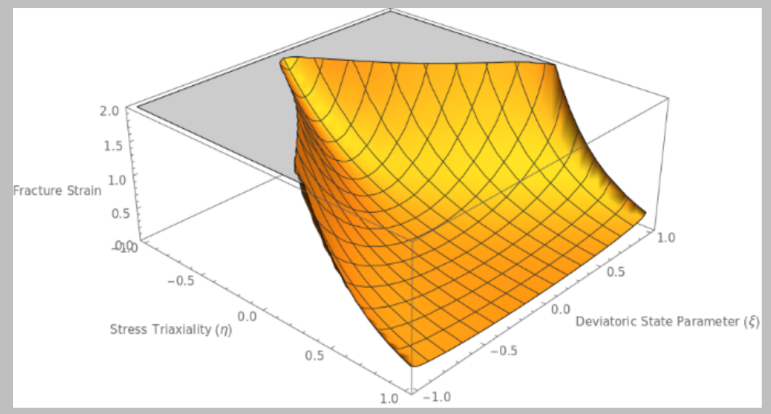 | 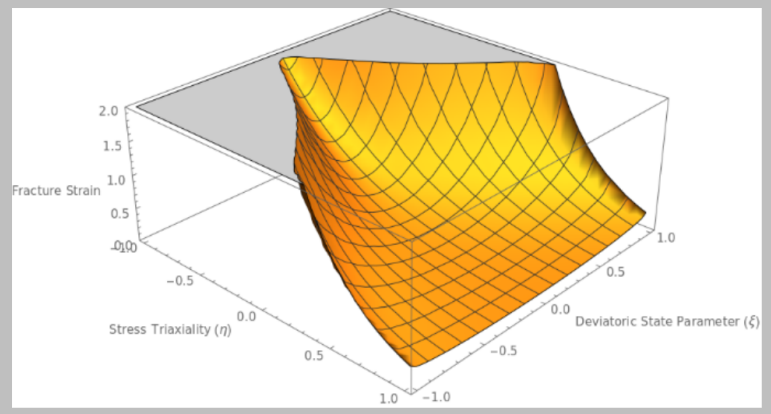 |
| -40 °C | 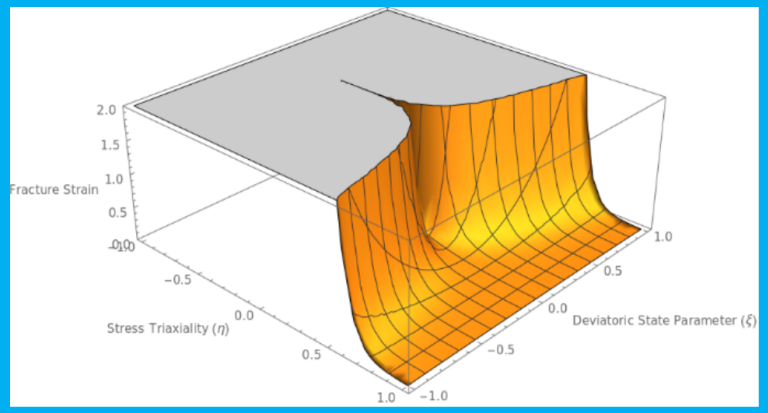 | 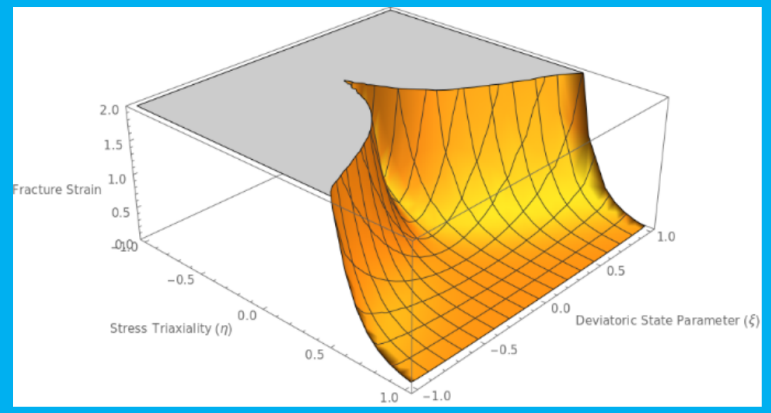 | 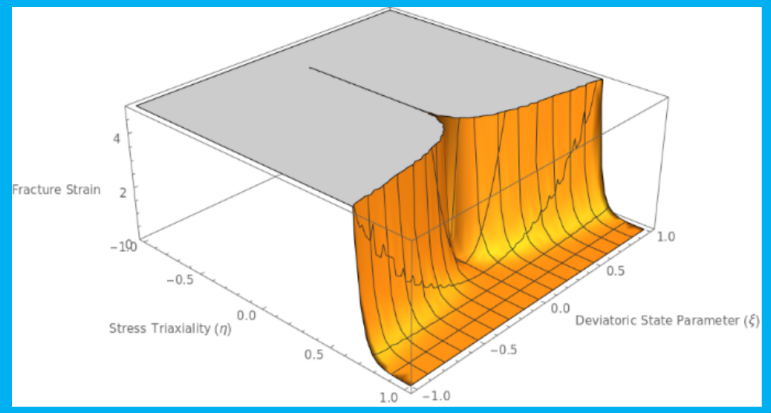 |

# Summary and Conclusions

- A X-W failure model has been developed for PH13-8Mo H950 steel @ 20 °C and -40 °C.
- Mechanical testing using five different test specimen geometries that vary in both stress triaxiality and deviatoric state parameter was conducted to collect the needed data.
- Unlike the other specimens tested, the 3 mm notch samples tested at -40 °C demonstrated features consistent with both ductile fracture and brittle cleavage, suggesting that the ductile-to-brittle transition temperature for PH13-8Mo H950 steel is near -40 °C.
- Finite element modeling was employed to extract the necessary information for the derivation of the X-W failure model parameter.
- It was observed that the assumed exponential relationship between stress triaxiality and fracture strain at a deviatoric state parameter value of 1 does not provide a good fit to all of the test data at -40 °C, indicating that the assumed exponential relationship may not be appropriate for this material at -40 °C.

# THANK YOU

# Biography – John Bignell

John Bignell has worked as a structural engineer in various roles for the past 17 years. In 2006 he graduated from the University of Illinois at Urbana/Champaign with a Ph.D. in Civil Engineering. His graduate coursework and research were focused on structural mechanics, finite element methods, and computational science. Following graduation, John joined the Spacecraft Structures and Dynamics group at NASA's Jet Propulsion Laboratory (JPL) where he was involved in the design and testing of portions of the Mars Science Laboratory (MSL) rover mission to Mars. In 2010, John joined the Structural and Thermal Analysis department at Sandia National Laboratories. During the next nine years he served in various roles, including as lead for the Radioisotope Power System Launch Safety (RPSLS) blast and impact team; lead structural analyst for the design, test, and certification of the first large capacity plutonium air transportation package; and modeling and simulation lead for the next generation of over-the-road transporter for government owned special nuclear material. In 2019, John left Sandia as part of a relocation to Colorado, at which time he joined the Structural Engineering Department at Ball Aerospace. At Ball, John served in a lead role overseeing the design, analysis, and test of various systems and components for a large satellite program. In 2022, John rejoined Sandia (this time virtually from Colorado) in the Packaging, Transportation, and Reactor Systems department where he serves in many of the same roles as he did previously.